Journal of the Taiwan Institute of Chemical Engineers 148 (2023) 104886

Contents lists available at ScienceDirect

Journal of the Taiwan Institute of Chemical Engineers

journal homepage: www.journals.elsevier.com/journal-of-the-taiwan-institute-of-chemical-engineers

Thermal management of a prismatic lithium battery pack with organic phase change material

Saeed Alqaed [a], Jawed Mustafa [a,*], Fahad Awjah Almehmadi [b], Mohsen Sharifpur [c,d,**]

[a] Mechanical Engineering Department, College of Engineering, Najran University, P.O. Box (1988), Najran, 61441, Saudi Arabia
[b] Department of Applied Mechanical Engineering, College of Applied Engineering, Muzahimiyah Branch, King Saud University, P.O. Box 800, Riyadh, 11421, Saudi Arabia
[c] Department of Mechanical and Aeronautical Engineering, University of Pretoria, South Africa
[d] Department of Medical Research, China Medical University Hospital, China Medical University, Taichung, Taiwan

ARTICLE INFO

Keywords:
Inlet and outlet position
Air-cooled
PCM
Lithium-ion battery

ABSTRACT

Background: This article examines a T-shaped lithium-ion battery pack (BPC) consisting of six prismatic cells using the finite element method (FEM). An optimal model is introduced for batteries' thermal management (THMT) by changing the position of the inlets and outlets.
Methods: The outlet is where the fully developed airflow leaves, and the walls use the no-slip boundary condition. The batteries are placed in an enclosure filled with phase change material (PCM) to create temperature uniformity on the batteries. The hydrodynamic and thermal modeling of airflow and the melting and freezing of PCM are performed in this study using the COMSOL program.
Significant findings: The results demonstrate that the batteries' maximum temperature (TMX) changes by changing the location of the inlets. Changing the position of inlets also affects the melting and freezing of the PCM, and better temperature uniformity on the batteries may be achieved using some models. The M4 model, in which the inlet and outlet are on the left and right sides, and an outlet is in the center, is the most appropriate model for industrial applications.

1. Introduction

Due to the depletion of fossil fuel supplies, rising oil prices, and environmental pollution, major automakers are now considering the development of electric cars [1,2]. To create and build electric and hybrid vehicles, many of these firms invest significant money each year in their research facilities [3,4]. The desire of automakers to build electric cars may be good news for the environment. However, there are still many doubts about the possibility of this amount of electric power and the power of the power grid to charge the batteries of this number of cars. Also, the amount of lithium available worldwide for making electric car batteries is another controversial limitation in this regard. However, the key difficulty is the electric energy proportionate to their operation [5–7]. Therefore, utilising rechargeable batteries has been the most common choice in this industry. The batteries of electric cars play a huge role in moving the car. They are designed in a tensile and very large way, which are the power source of electric cars' electric motor. The expansion of the use of electronic equipment has led to the need for energy storage and the necessity of using rechargeable batteries [8,9]. Due to the significant advantages of lithium-ion batteries, such as their high voltage, high mass and volume energy density, lack of memory effect, low self-discharge rate, ability to charge quickly, acceptable life cycle, and wide operating temperature range, their use has increased [10–12].

However, managing the battery's temperature, which significantly influences both the battery's performance and safety, is the most significant difficulty facing batteries. Therefore, a significant focus of researches has been devoted to solving the problems caused by the generation of heat in the battery assembly and various cooling methods by modeling or performing tests on the battery [13–15]. Active and passive cooling techniques are divided into two categories. The disadvantage of active approaches is the system complexity and need for an external energy source. Hence, the passive methods based on PCMs have been gradually taken into consideration [16,17]. According to the operating temperature range of batteries, paraffin has been an important

* Corresponding author at: Mechanical Engineering Department, College of Engineering, Najran University, Kingdom of Saudi Arabia.
** Corresponding author at: Department of Mechanical and Aeronautical Engineering, University of Pretoria, South Africa.
E-mail addresses: jmmustafa@nu.edu.sa (J. Mustafa), mohsen.sharifpur@up.ac.za (M. Sharifpur).

https://doi.org/10.1016/j.jtice.2023.104886
Received 10 March 2023; Received in revised form 16 April 2023; Accepted 17 April 2023
Available online 30 April 2023

Nomenclature

a	specific interfacial area
A_c (m^2)	The cross-sectional area
c_{pb} (J $kg^{-1°C-1}$)	Heat capacity
c	salt concentration
D	salt diffusion coefficient
Ds	lithium diffusion coefficient
F (C mol-1))	Faraday's constant
R (Ωm-3)	Internal resistance
I (A)	Discharging current
p_{drop} (Pa)	Pressure drop of air through the channel
T_b (°C)	Temperature in battery units
E_{oc} (V)	Open circuit voltage
i (A)	Discharging current per unit volume
n	Number of electrons participating
v (m s^{-1})	Air flow velocity
P_c (W)	Power loss
V (V)	Voltage
S_{ab} (W m^{-3})	Heat absorption rate
S_T (W m^{-3})	Source term
SOC	State of charge
k_b (W $m^{-1°C-1}$)	Thermal conductivity of battery materials
T_a (°C)	Temperature of air
k_a (W $m^{-1\ °C-1}$)	Thermal conductivity of air
c_{pa} (J $kg^{-1\ °C-1}$)	Specific heat capacity of air
p(Pa)	Static pressure
t	time

Greeks

Λ (m^3)	Volume of battery
ΔS (J mol^{-1} K^{-1})	Entropy change
ρ_b (kg m^{-3})	Density of battery materials
ϵ	volume fraction
η	electrode potential

category of PCMs in the field, which has caused a lot of research to improve their thermal conductivity [18]. Passive THMT systems improve the rate of melting or freezing of the PCMs compared to active ones, which makes the system more efficient. The cost and complexity of the hybrid systems and the need for optimization are some challenges of these systems [19,20].

An experimental investigation was undertaken by Xie et al. [21] to determine how copper foam and fins affected the efficiency of PCM heat transfer. The copper foam's porosity was 96%, the fin's thickness was 0.8 mm, and the PCM's characteristics were 99%. One sample composed of fin, copper foam, and paraffin, and the other without fins, were arranged horizontally and vertically (the fins had a tree or zigzag arrangements). They were under different heat fluxes and their temperature changes were assessed. The findings demonstrated that using copper foam and fins together increases thermal conductivity and melting rate by up to 2.7 times by conduction heat transfer along the fin. Also, the horizontal arrangement had a greater contribution to heat transfer than vertical one in composites with higher thermal conductivity. Mousavi et al. [22] evaluated and optimized lithium batteries with an air-cooled cooling system of a BPC containing 150 cylindrical lithium-ion battery cells (BTTC) in a PVC enclosure. Their findings showed that increasing the diameter of the tubes mounted on the battery

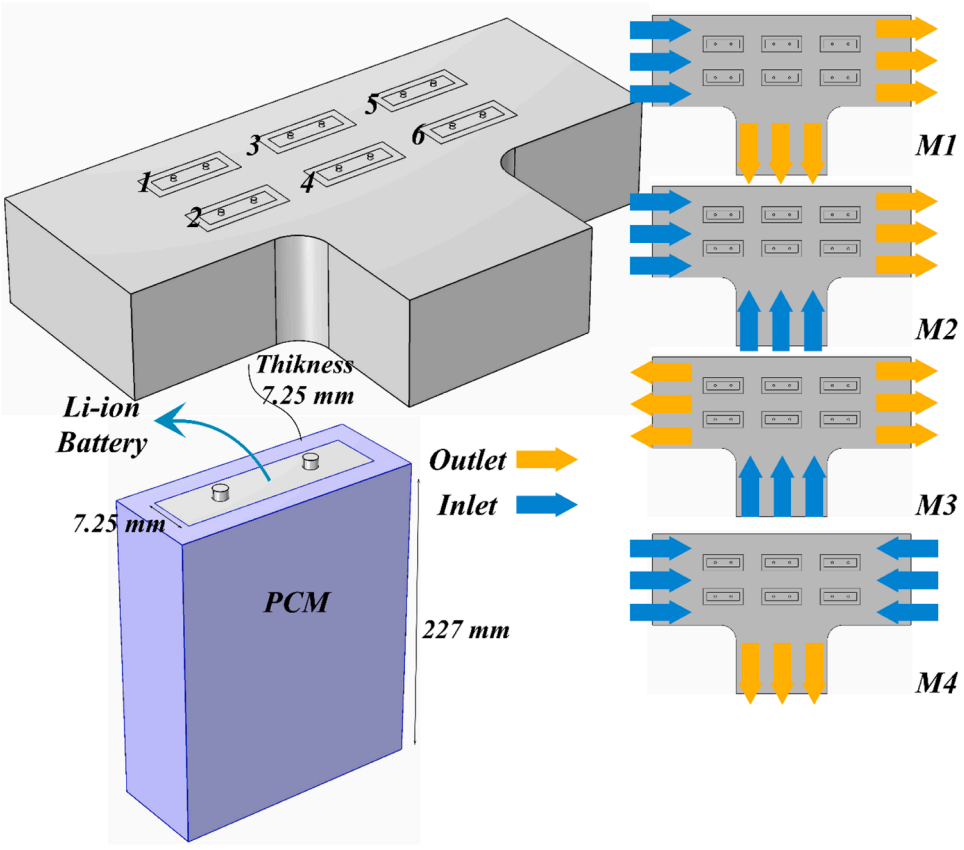

Fig. 1. Schematic of battery Thermal management. (Air and PCM).

Table 1
Equations governing the flow of PCM [29].

$\rho c_p \frac{\partial T}{\partial t} + \rho c_p \vec{u}.\nabla T = \nabla.(k\nabla T)$	Energy equation for liquid phase
$\rho c_p \frac{\partial T}{\partial t} - \nabla.(k\nabla T) = 0$	Energy equation for solid phase
$\rho \frac{\partial \vec{u}}{\partial t} + \rho(\vec{u}.\nabla)\vec{u} - \mu.\nabla^2\vec{u} = -\nabla P + \vec{F}_b + \vec{F}_a$	General form of energy equation with surface and volume forces
$\vec{F}_b = -\rho_{liquid}(1 - \beta(T - T_m)).\vec{g}$	Body forces
$\vec{F}_a = -A(T).\vec{u}$	Surface forces
$A(T) = \frac{C(1-B(T))^2}{(B^3(T)+q)}$	Karman-Kozeny relation for porous media
$\nabla P = \frac{-C(1-B(T))^2}{B^3(T)}.\vec{u}$	Darcy law
$\vec{u} = -\frac{K}{\mu}\nabla P$	velocity
$B(T) = \begin{cases} 0, & T < (T_m - \Delta T) \\ (T - T_m + \Delta T)/2\Delta T, & (T_m - \Delta T) \le T < (T_m + \Delta T) \\ 1, & T > (T_m + \Delta T) \end{cases}$	$B(T)$

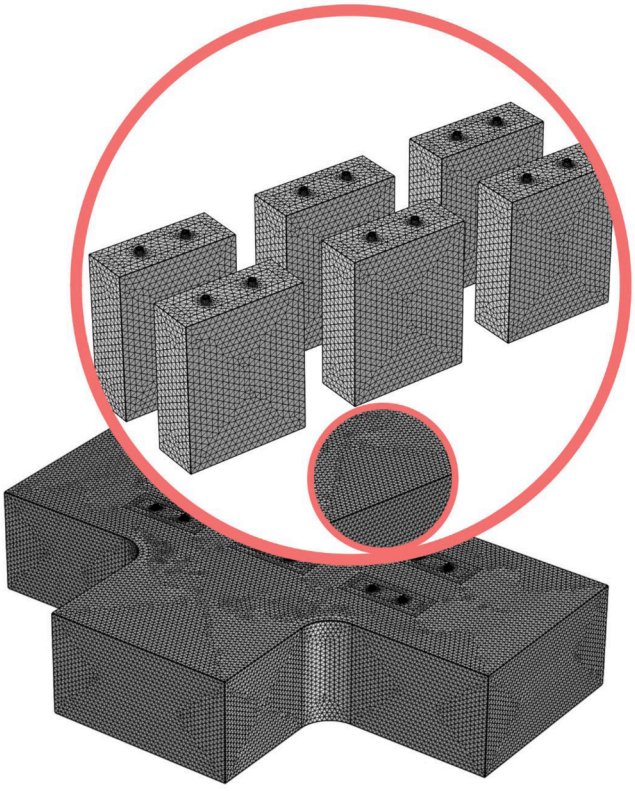

Fig. 2. The grid employed for the present geometry.

and maintaining a certain range of air velocity (V-air) may increase the Number of Transfer Unit. A battery THMT system with U-shaped microchannels and air-filled heat pipes was evaluated by Ren et al. [23]. According to their research, for charging currents of 2C and 3C, respectively. Even in conditions of high charge and discharge, the cooling method performed exceptionally well for THMTs. Chen et al. [24] looked into how PCMs affected the THMT of an air-cooled lithium battery system. Their findings shown that, particularly at high ambient temperatures, the active air-cooled technique had a superior cooling effect than the PCM-cooled one. However, the active air-cooled method produced increased temperature non-uniformity at low intake V-air. In comparison to PCM cooling, the air-cooled battery module had a longer cycle life. The two approaches were also contrasted using cyclic cost, a

Table 2
The grid independence test for the geometry consisting of PCM, air, and lithium batteries

	300000	400000	500000	600000	700000
T	298.96	298.68	298.51	295.50	298.50

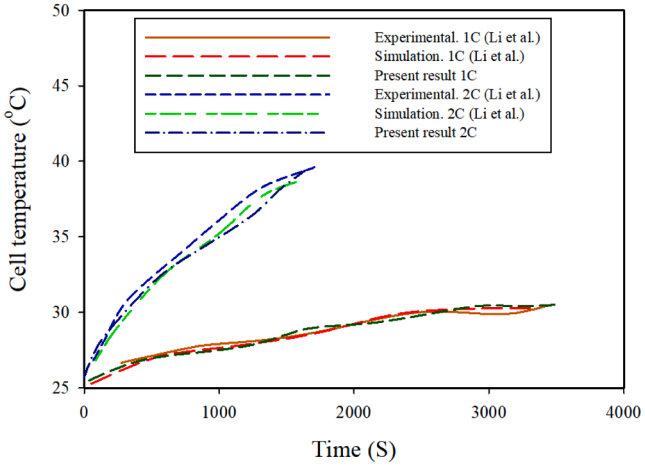

Fig. 3. Comparison of the results, including the TOBT surface, obtained from the present work and reported by Li et al. [36].

recently suggested assessment indicator.

Thermal management of the battery using passive cooling systems is effective up until the point where the PCM melts completely. After that, the system is unable to control the battery's temperature. As a result, the passive method, which uses PCM, is only effective for a brief time while requiring no energy. On the other hand, external energy is needed for the active methods; but they can be utilized all the time. Using the hybrid methods, i.e. the use of both active and passive ones, can eliminate their drawbacks to a large extent. It is possible to utilize the passive method at a certain time when there is no need for energy to manage the battery temperature. When the PCM is completely melted, the battery temperature is controlled and the PCM is completely solidified by using the active method. Then, the passive method can be employed again. The heat generated by batteries is numerically modeled in the current work, and a hybrid active-passive cooling system is created and simulated for their THMT [25,26]. The forced airflow passing through a heatsink is used as active cooling, and a PCM with a suitable melting temperature is used to cool the batteries as passive cooling. The innovations of this work are to use PCM in the enclosure around the batteries and the changes in the inlet and outlet position. The variations in temperature and the system performance are examined and an optimal model is presented.

2. Problem description

The BPC considered in the present work is shown in Fig. 1, indicating the position of the inlet and outlets. Six prismatic batteries are placed inside the T-shaped channel. Airflow and PCM are employed for the THMT of lithium batteries. The airflow that has a temperature and velocity that are both constant enters the channel, and the airflow that has completely developed escapes from the opposite side. After the container has been filled with PCM, lithium prismatic batteries are inserted inside it.

The battery's electrochemical model is shown in the example below. The basic mathematical model of the battery is presented here, while Ref. [27] provides further information on the parameters and reaction kinetics. The division of the model into many parts, including a

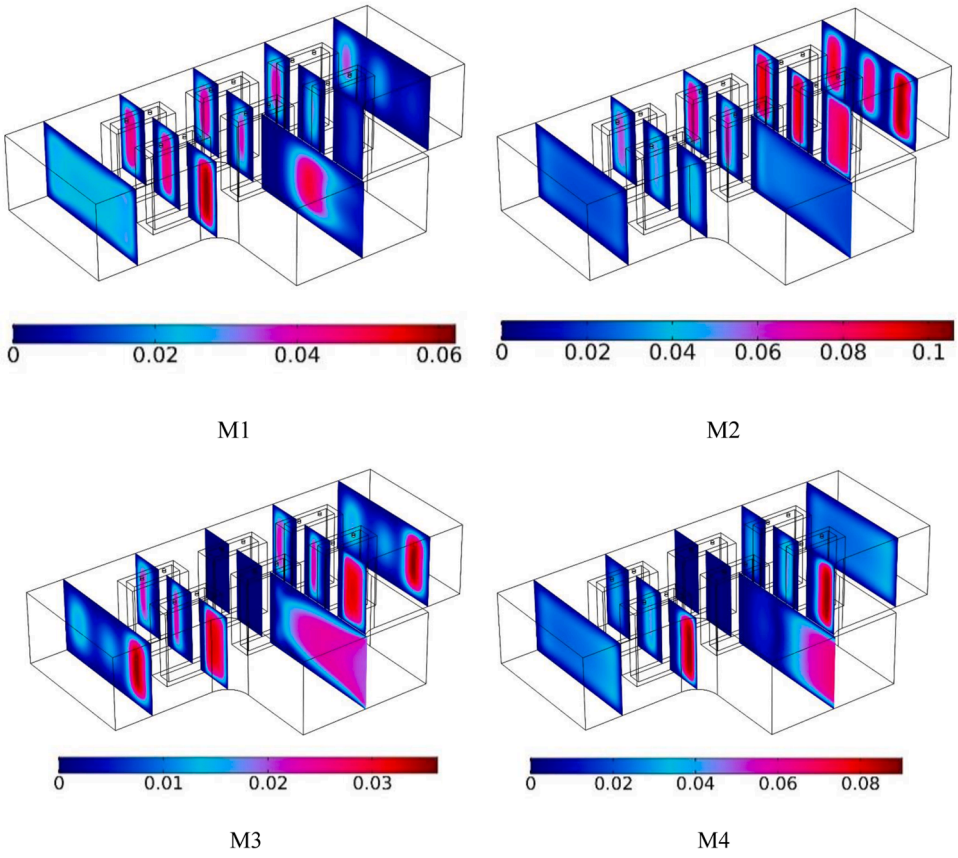

Fig. 4. V-air (m/s) in the BPC in various cross-sections for different inlet and outlet models.

separator area in the center and two composite electrodes on each side, is analogous to how lithium batteries are made. The equations below may be used to explain the solution phase of the composite electrode [3, 28,29]:

$$\epsilon\frac{\partial c}{\partial t} = \nabla\cdot(D\nabla c) - \frac{i_2\cdot\nabla t_+^0}{F} + aj_n\left(1+t_+^0\right) \tag{1}$$

$$i_2 = -k\nabla\phi_2 + \frac{2kRT}{F}\left(1+\frac{\partial lnf_\pm}{\partial lnc}\right)\left(1-t_+^0\right)\nabla\ln c \tag{2}$$

$$aj_n = \frac{1}{F}\nabla\cdot i_2 \tag{3}$$

The solid phase equations' description of composite electrodes is provided here [30,31]:

$$i_1 = -\sigma\nabla\phi_1 \tag{4}$$

$$\frac{\partial c_s}{\partial t} = D_s\left[\frac{\partial^2 c_s}{\partial r^2} + \frac{2}{r}\frac{\partial c_s}{\partial r}\right] \tag{5}$$

The energy balance for a battery may be used to determine the three-dimensional temperature distribution that takes place within a battery throughout the charging, discharging, and resting phases of its operation [3,29,32]:

$$\frac{\partial}{\partial t}\left(\rho_a c_{p,b} T_a\right) = \nabla\cdot(k_b\nabla\ T_a) + \dot{Q}_{gen} \tag{6}$$

Because the battery is made up of several layers composed of various materials, its heat conductivity is not uniform in all directions and is thus anisotropic. The battery's axial thermal conductivity has a greater active portion than its radial portion. The following is a list of the heat conductivities that the active component of the battery has in both the radial and axial directions [3,29]:

$$k_{b,r} = \frac{\sum L_i}{\sum\left(\frac{L_i}{k_i}\right)} \tag{7}$$

$$k_{b,Z} = \frac{\sum(L_i\times k_i)}{\sum L_i} \tag{8}$$

$$C_{p,b} = \frac{\sum\left(L_i\times C_{p,i}\right)}{\sum L_i} \tag{9}$$

$$\rho_b = \frac{\sum(L_i\times\rho_i)}{\sum L_i} \tag{10}$$

The rate of heat generation by the battery, which is represented by the last component on the right side of Eq. 10, is the factor that has the most influence on the three-dimensional temperature distribution that exists inside the battery. The battery's active component creates two forms of heat: heat from electrochemical reactions and heat from the battery's internal resistance to current flow [3,33]. The formula for calculating the heat produced by the active component of the battery is as follows:

$$\dot{Q}_{gen} = \dot{Q}_{ec} + +\dot{Q}_J = -T\Delta s\frac{I}{nF} + I(E-V) \tag{11}$$

The following equations, respectively, govern continuity, momentum, and energy [34]:

$$\frac{\partial\rho_p}{\partial t} + \nabla\cdot(\rho_a\overrightarrow{v}\ ) = 0 \tag{12}$$

$$\frac{\partial}{\partial t}(\rho_a\overrightarrow{v}) + \nabla\cdot(\rho_a\overrightarrow{v}\ \overrightarrow{v}\ ) = -\nabla P + \rho g \tag{13}$$

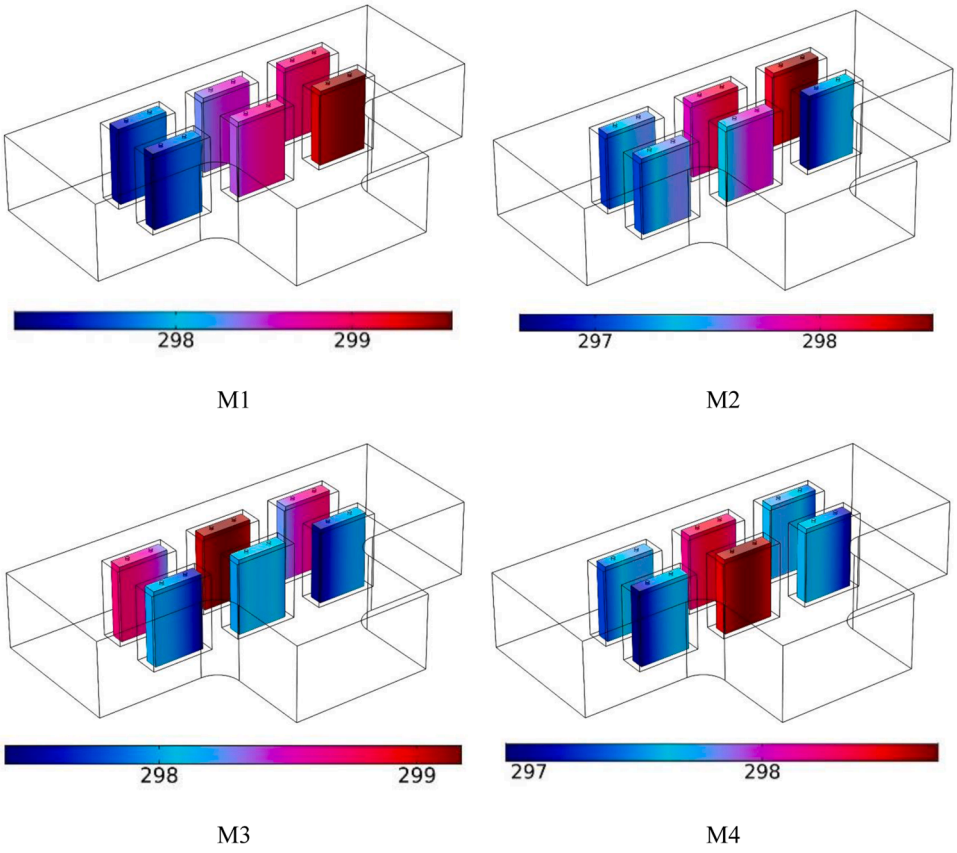

Fig. 5. TOBT cells (K) for different inlet and outlet models.

$$\frac{\partial}{\partial t}\left(\rho_a c_{p,a} T_a\right) + \nabla\cdot\left(\rho_a c_{p,a}\vec{v}\ T_a\right) = \nabla\cdot\left(k_a \nabla\ T_a\right) \tag{14}$$

The following is an expression of the energy conservation equation that applies to the nano-PCM.

The equations are shown here in Table 1.

Therefore, $B(T) = 0$. The value of the function $B(T)$ can be written as follows: the function $B(T)$ is enhanced linearly from zero to one between two PCM phases [35].

3. Numerical method and grid study

In this study, COMSOL software is used to simulate the hydrodynamic and thermal aspects of airflow as well as the melting and freezing of PCM. The grid is an unstructured one and the solution method is the FEM. The FEM divides the computational domain into smaller and simpler elements, then the equations are solved for each element. The geometry of airflow, lithium battery, and PCM are meshed separately on them. A finer mesh is used in the vicinity of walls. One of the factors affecting the accuracy of the numerical solution is the number of elements used in the computational domain. In COMSOL software, it is possible to create a smart grid in the computational domain by determining the minimum and the maximum length of the elements, so that the grid is finer next to the walls. The grid created using the explored geometry is shown in Fig. 2.

The computational domain involves 300000 to 700000 elements, while the minimum and maximum length of the elements is 0.02 to 0.8 mm, respectively. According to Table 2, when the number of elements is higher than 500000, there are very small changes. As the battery surface temperature is unaffected by increased components, the grid with 500000 elements is used for the simulations. The computational equations are solved using the GMRES technique. The simulation time is about 21 hours for each run using a system with 32GB of RAM and an "Intel(R) Core(TM) i7" CPU.

4. Validation

Validation of numerical simulations is crucial, and the numerical results must be compared with other similar data. For this reason, the outcomes of the current simulations are contrasted with those of Ref. [36], a study that is highly similar to the present work. The battery's temperature readings (TOBT) and the researchers' findings coincide quite well. Li et al. [36] examined the temperature and battery life using some physics in their solution. This study examined a lithium-ion battery pack placed in an air channel numerically and experimentally. The temperature of each cell of the battery pack is analyzed separately. They employed experimental data to validate the numerical model and used it as an index for numerical results. This comparison is performed for two different battery charge rates, i.e. 1C and 2C, at different times. Experimental and numerical results have been compared with the previous papers and the present article using these charge rates. They considered several cooling methods. In this comparison, the TOBT surface is examined. The highest error, as shown in Fig. 3, is 4.8%, and the findings from the current simulations are quite accurate.

5. Results and discussion

Fig. 4 illustrates the V-air in the BPC in various cross-sections for different inlet and outlet models. The velocity values between the batteries depend on the location of the inlet and outlets. Due to the top and bottom walls and the created flow produced by traveling along the inlet, the V-air is amplified in the center of the channel on the air inlet side. The airflow branches reach each other in the middle of the pack and exit from the BPC. The velocity of the airflow between the BTTCs in some

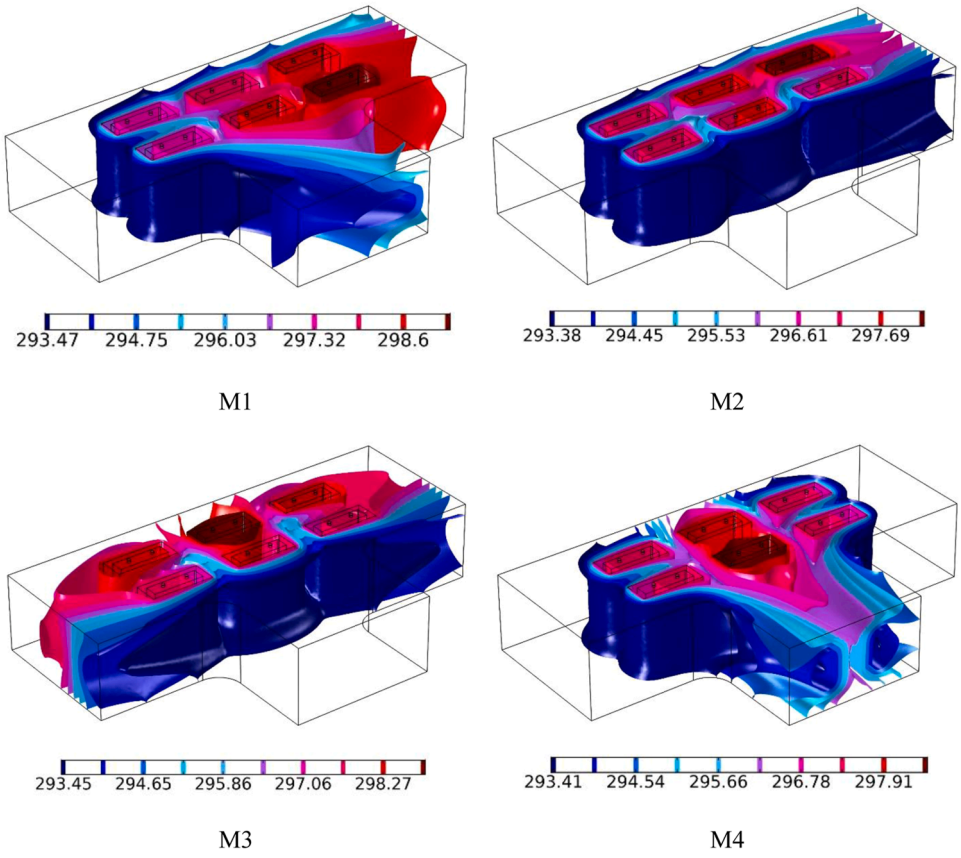

Fig. 6. Isothermal planes in the pack (K) for different inlet and outlet models.

parts is maximum. The cooling is better in these parts because of the high V-air. On the other hand, the amount of cooling of the batteries and PCM is low in the parts where the airflow velocity is low. The highest maximum V-air occurs in M2 and the lowest maximum air temperature corresponds to M3. The area where the highest V-air occurs and the battery is more effectively cooled changes depending on where the inlet and exit are located. In most models, the batteries placed in the front row are at a higher V-air than those in the back row.

Fig. 5 depicts the TOBT cells for different inlet and outlet models. Changing the location of the inlet and outlets affects the TOBT cells. The BTTCs are supposed to be on the cooler side of the air inlet, and the batteries are on the higher temperature side of the outlet. For M1, the batteries on the right side of the BPC have the TMX whereas the batteries on the left are the coolest. This TOBT is lower because of the air on the left. For M2, the front row battery on the right side of the BPC and the batteries on the left side of the pack are both warmer than the rear row battery on the same side of the BPC. This TOBT is the lowest due to the airflow in this area. For M3, the middle battery in the rear row is at a high temperature while the batteries in the front row are at a lower temperature. The front side of the BPC's air circulation causes the temperature to even out. The similar circumstance is present in M4. The right and left batteries of the BPC of the M4 have a lower temperature than the central ones, and the outlet is located in the centre of the pack.

Fig. 6 demonstrates the isothermal planes in the pack for different inlet and outlet models. The isothermal planes are shown from the inlet side towards the outlets. For M1, the planes are drawn toward the middle and right outlets of the BPC from the left side inlet where the air enters the BPC. For M2, the air enters from the left side, and in the middle of the BPC exits from the right side of the BPC. For M3, the air enters the middle of the BPC and leaves from both sides of the BPC. For M4, the air enters from the left and right sides of the BPC and exits from the middle of the BPC. This model and M3 have symmetrical isothermal planes. The density of isothermal planes is higher on the BTTCs where the heat transfer is more and the temperature difference is higher. The batteries on the air side are at a lower temperature and the air around the batteries that are at a higher temperature has a higher temperature.

Fig. 7 illustrates the air streamlines with velocity and temperature colors on the enclosure around the BTTCs for different inlet and outlet models in 2000, 4000, and 6000 s. On one side of the BPC that air enters, the amount of volume fraction of molten PCM is lower and on the side of the outlets, the amount of molten PCM around the battery is higher depending on the model. At the time 2000 s, there is a quantity of molten PCM around the hot batteries. The PCM is in the solid phase around the batteries with a lower temperature. At the time of 4000 s, most of the PCM melts, and only a few parts of the PCM around the batteries remain solid at the inlet. At the time of 6000 s, all the PCM is in the solid phase and it is not melted around the batteries. Air temperature also depends on the amount of liquid or solid PCM. In cases where there is more molten PCM around the batteries, the air temperature is a little higher. For M3 and M4, the airflow and the growth of the melting and freezing front of the PCM are symmetrically related to the middle of the BPC due to the symmetrical boundary conditions of the BPC. In each BTTC, the

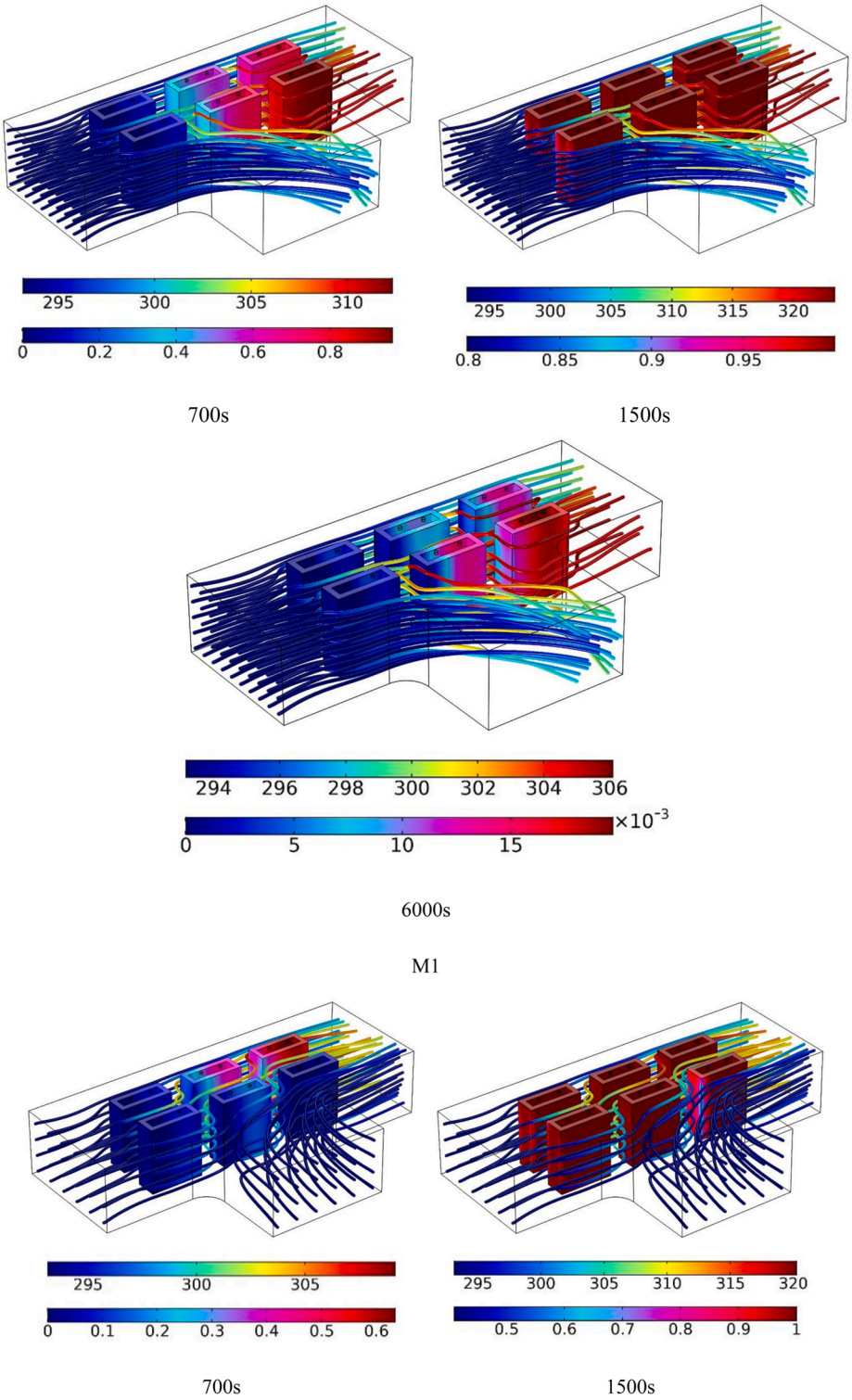

Fig. 7. Air streamlines (K) with velocity and temperature colors on the enclosure around the BTTCs for different inlet and outlet models in 2000, 4000, and 6000 s.

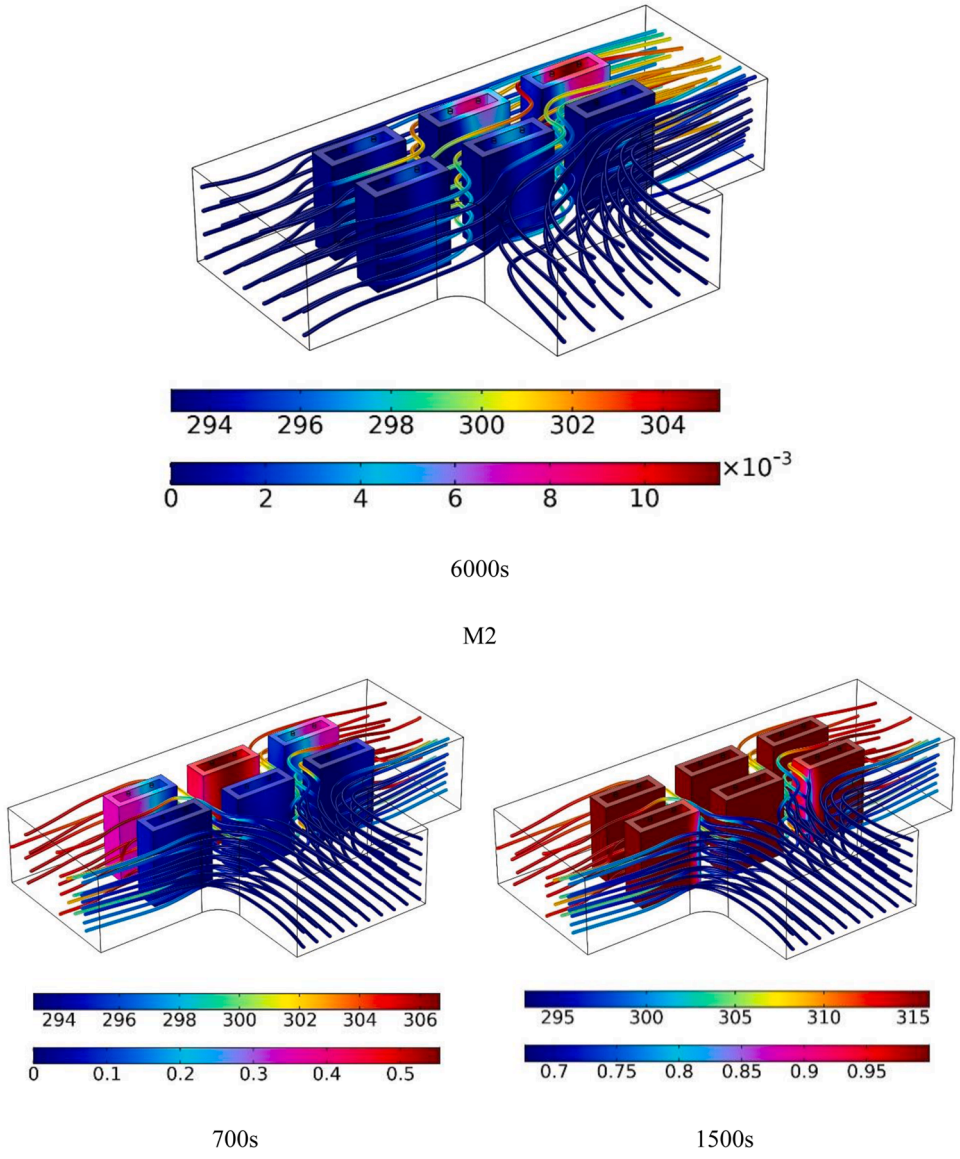

Fig. 7. (*continued*).

TOBT cell may be different depending on which part of the PCM is solid and which part is liquid.

Fig. 8 demonstrates the mid TOBT for different inlet and outlet models up to 6000 s. The temperatures shown in the figures indicate the average temperature of each battery cell. The instantaneous temperature changes of the batteries show that the TOBTs are highly dependent on time due to the presence of PCM. There is an initial enhancement in the temperature of all BTTCs and then, a temperature jump occurs on the batteries so that the TOBT reaches its maximum value at this time. After this time, the TOBT is reduced so that the TOBTs become lower over time. At first, the TOBTs are reduced with a rapid trend, but the decreasing trend of the temperature becomes slower with time until a constant decreasing trend occurs. The TOBT reaches its maximum value of more than 330 K. At 6000 s, the TOBT reaches less than 310 K. The presence of the TOBT control systems, including airflow and PCM, affects their temperature. These changes result from PCM melting and freezing control systems and airflow. This process generally occurs on the TOBTs, and changing the location of the inlet and outlets changes the trend of the TOBT only when the temperature drops. By changing the locations of the air outlets, one or two of the cells are placed on the air inlet or outlet sides each time. Due to the lower temperature of the air at the inlet compared to other parts of the BPC, the cell that is placed on the side of the air inlet becomes cooler and faster cooling occurs when the TOBTs are decreasing. Also, the BTTCs on the airflow's upstream side have a lower TMX in the BPC. On the other hand, the BTTC or batteries that are placed close to the outlets have a higher TMX and their cooling process takes place slower. As the air near the outlet is warmer than the surrounding areas, less heat is lost there, resulting in a slower cooling rate.

The temperature values on the BPC for various inlet and outlet models up to 6000 s are shown in Fig. 9. The average temperature of the battery pack is calculated from the temperature of each cell. The average

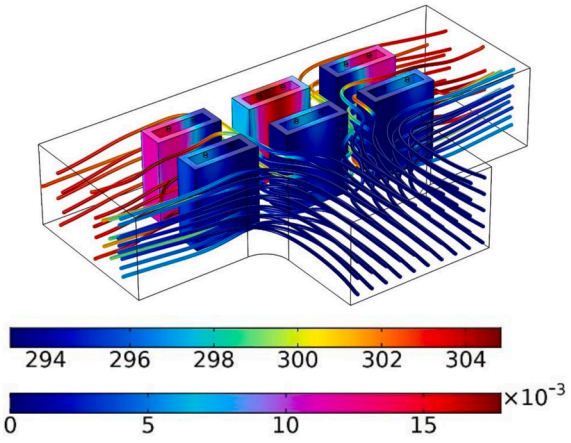

6000s

M3

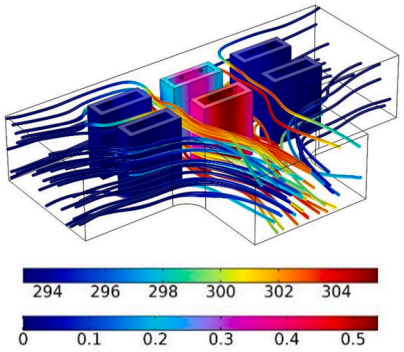

700s

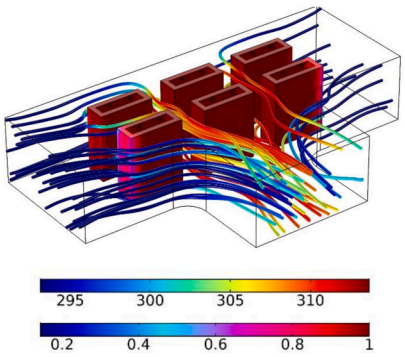

1500s

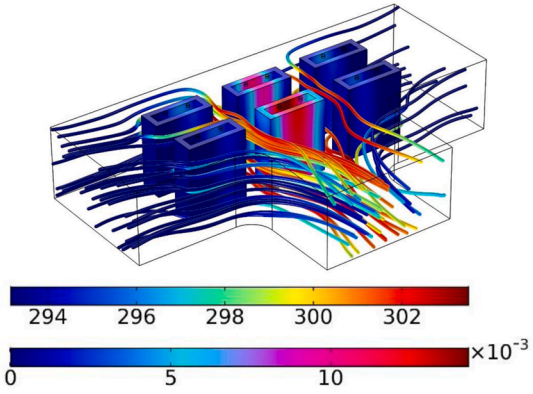

6000s

M4

Fig. 7. (*continued*).

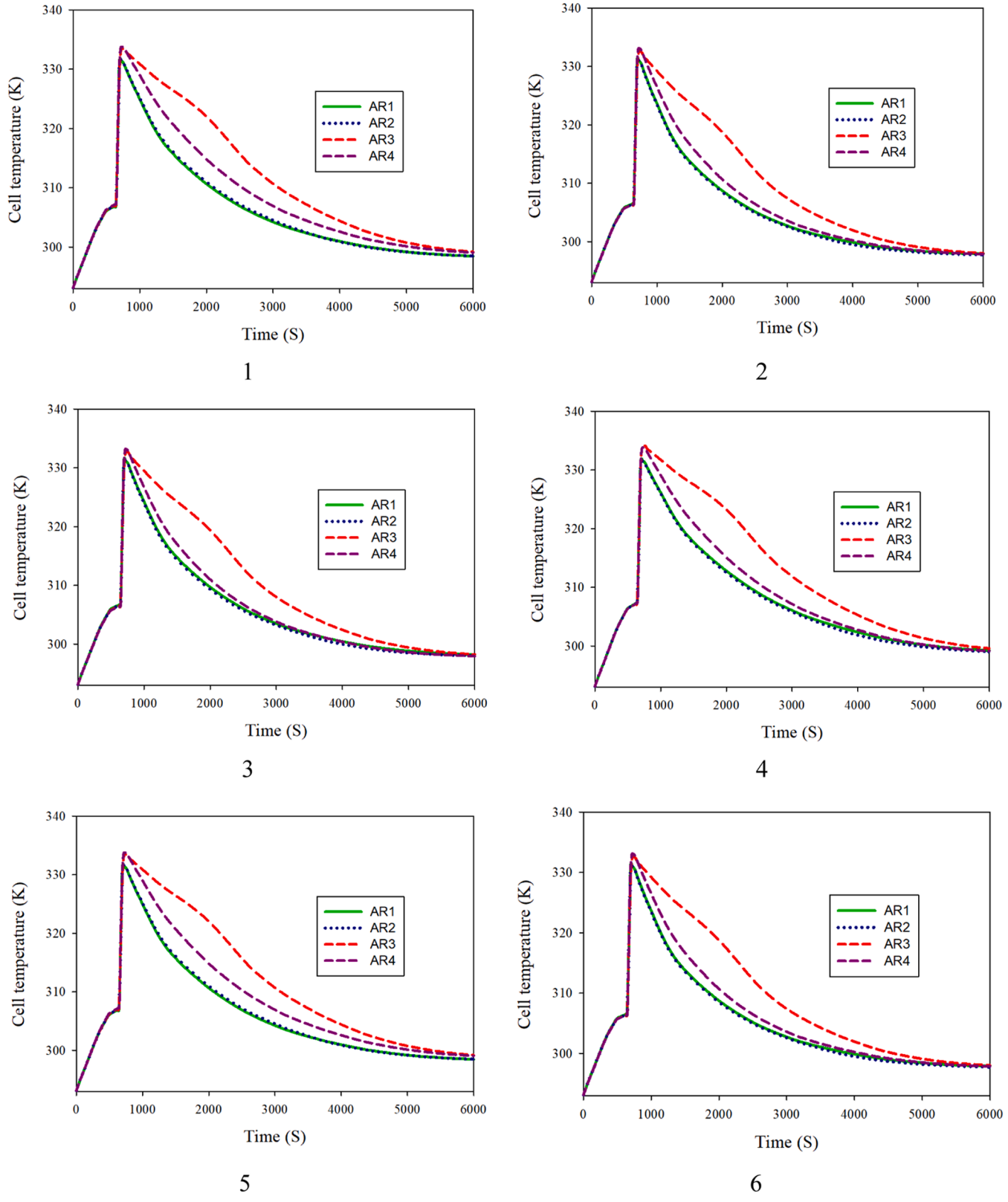

Fig. 8. Mid TOBT values for different inlet and outlet models up to 6000 s.

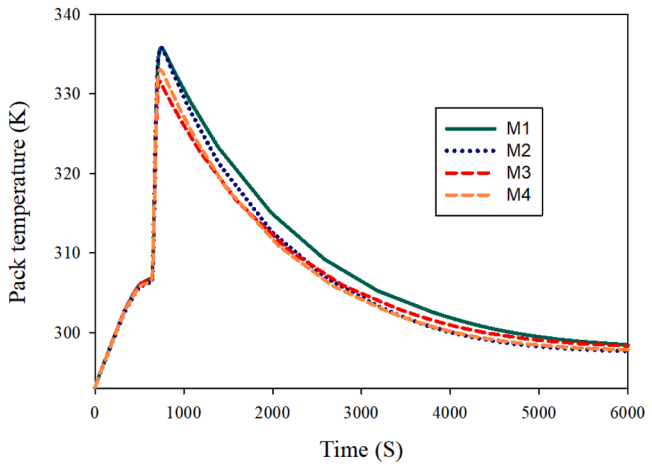

Fig. 9. Temperature values on the BPC for different inlet and outlet models up to 6000 s.

temperature of the battery pack has been calculated by averaging the temperatures of six battery cells, which is how the surface temperatures of battery cells are obtained. The BTTCs' collective behavior affects the BPC's overall behavior, and the BTTCs' collective temperature behavior affects the BPC's behavior with regard to temperature. The PCM melting and freezing around the batteries affects the BPC's behaviour at different temperatures. In the beginning, due to the lack of airflow in the entire BPC and the complete melting of the PCM around the batteries, the temperature of the BPC is enhanced and reaches above 330 K for different models. After this time, depending on the model, the temperature of the BPC is decreased with a faster or slower trend to reach less than 300 K. Changing the inlet and outlet model affects the TMX reached by the BPC and the temperature trend up to 6000 s. The temperature of the BPC for different models eventually becomes close to each other. The TMX in the BPC occurs between 720 and 740 s, which is the maximum value for M2 and the minimum value for M4. The temperature difference between these two models in the TMX is 1.88 °C. During the cooling of the BPC, M1 has a TMX in the period from 700 to 6000 s, and M1, M2, or M3 have a minimum temperature at different times.

Fig. 10 depicts the volume fraction of molten PCM around BTTCs for different inlet and outlet models up to 6000 s. The melting and freezing process of PCM in different BTTCs is very similar to each other. Changing the inlet and outlet locations have a different effect on different cells. When the cooling process starts in the batteries, temperature increases due to the lack of airflow in the BPC. Since the TOBT does not reach the melting temperature of the PCM, the melting process does not occur. After this time, the freezing process of the PCM starts, and the TOBTs are decreased due to the flow of air in the BPC. Because of the collision of cold air with the PCM, all the PCM becomes solid again in a short time. After this time, all PCM remains solid due to the small volume of PCM used. The change of the model does not have much effect on the PCM freezing time, like cells No. 1, 2, and 4. However, on some other BTTCs, such as cells No. 3, 5, and 6, it greatly affects the freezing process of PCM. By changing the location of the inlet and outlets, the PCM that surrounds the cells located on the inlet side is solidified in a shorter time. The PCM that surrounds the cells located on the outlet side needs more time for freezing. The fastest PCM freezing process occurs in BTTC No. 3, for M 4. The longest PCM freezing process occurs for M1. M3 has faster PCM freezing and M1 has the longest time for PCM freezing in BTTC No. 5.

The volume percentage of molten PCM in the BPC for various input and output models up to 6000 s is shown in Fig. 11. To determine the volume percentage of molten PCM at any given moment, the quantity of molten PCM in the battery cell is averaged. To express the average value of the molten PCM in the battery pack, the average value for each battery cell is averaged again to finally calculate the volume fraction of the molten PCM in the battery pack. All the PCM in the BPC melts in a short time, and the PCM remains molten for a time of about 1000 s. After this time, depending on the model of the inlet and outlets, the PCM freezing process starts. In a relatively limited time, all the PCM becomes solid again. The PCM freezing process is finally completed for all models before 3500 s and the PCM remains solid for the rest of the time. In the beginning, due to the lack of airflow in the BPC due to its very low velocity and the small volume of PCM used around the batteries. After a while, the PCM freezing process starts due to the airflow around the batteries. Air cooling causes all PCM to be converted to the solid phase. Changing the inlet and outlet locations affects the freezing time of the PCM. M4 requires the minimum time for the complete solidification of PCM, and M1 needs the maximum time. M1 has a two-minute delay in completely freezing the PCM compared to M4. During the freezing time, the minimum and maximum amount of solid PCM corresponds to M1 and M4, respectively.

6. Conclusions

A three-dimensional numerical study is performed on the THMT of a T-shaped BPC using PCM and laminar airflow in the BPC. The batteries are prismatic lithium-ion type, and PCM is used around them. The BPC has three inlets and outlets. The input and output locations are altered, and this investigation is completed in 6000 s.

1- The TMX in the BPC occurs between 720 and 740 s, which is the maximum value for M2 and the minimum value for M4. The temperature difference between these two models in the TMX is 1.88 °C.
2- During the cooling of the BPC, M1 has a TMX in the period from 700 to 6000 s, and M1, M2, or M3 have a minimum temperature at different times.
3- Changing the inlet and outlet positions does not significantly impact PCM cooling time for BTTCs No. 1, 2, and 4, but it greatly impacts PCM freezing time for BTTCs No. 3, 5, and 6.
4- Changing the inlet and outlet locations affects the amount of time for the complete freezing of PCM. M4 requires the minimum time for the complete solidification of PCM, and M1 needs the maximum time. M1 has a two-minute delay in completely freezing the PCM compared to M4.
5- During the freezing time, the minimum and maximum amount of solid PCM corresponds to M1 and M4, respectively.

Declaration of Competing Interest

The authors declare that they have no known competing financial interests or personal relationships that could have appeared to influence the work reported in this paper.

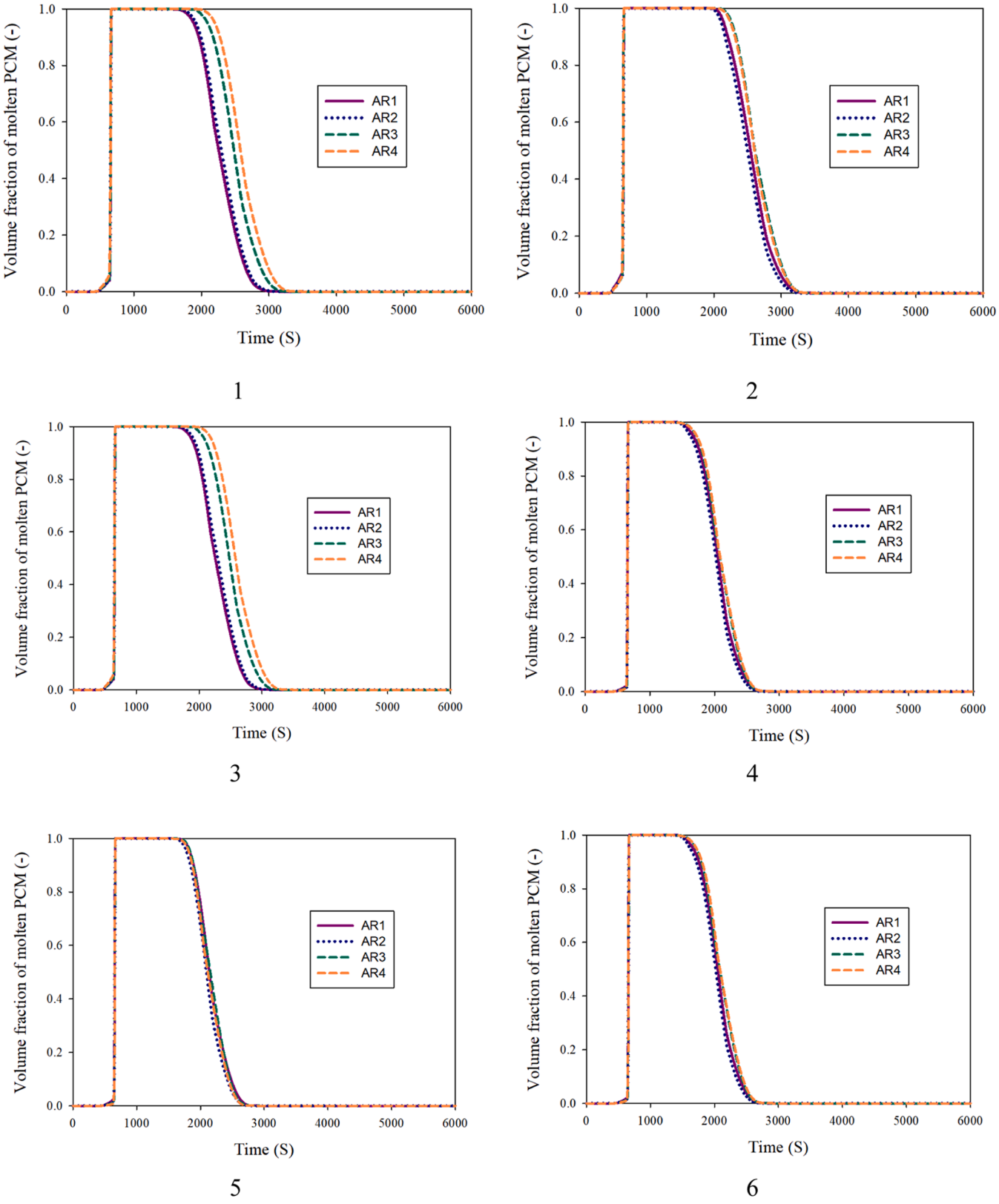

Fig. 10. The volume fraction of molten PCM around BTTCs for different inlet and outlet models up to 6000 s.

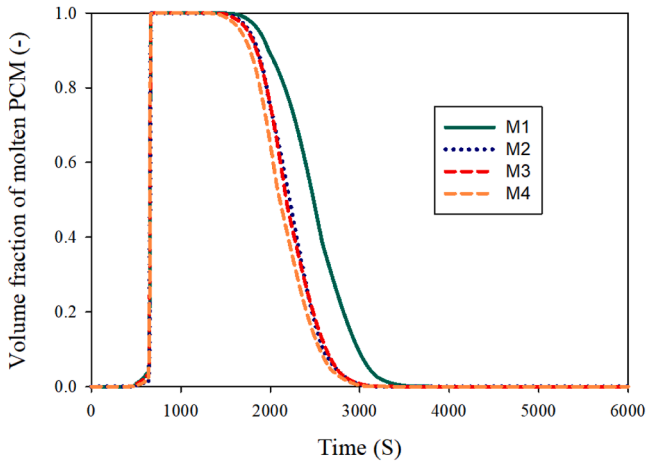

Fig. 11. Volume fraction of molten PCM in the BPC for different inlet and outlet models up to 6000 s.

Acknowledgements

Authors would like to acknowledge the support of the Deputy for Research and Innovation Ministry of Education, Kingdom of Saudi Arabia for this research through a grant (NU/IFC/2/SERC/-/22) under the Institutional Funding Committee at Najran University, Kingdom of Saudi Arabia.

References

[1] Sohani A, Shahverdian MH, Sayyaadi H, Samiezadeh S, Doranehgard MH, Nizetic S, Karimi N. Selecting the best nanofluid type for A photovoltaic thermal (PV/T) system based on reliability, efficiency, energy, economic, and environmental criteria. Journal of the Taiwan Institute of Chemical Engineers 2021;124:351–8.
[2] Martins LS, Guimarães LF, Botelho Junior AB, Tenório JAS, Espinosa DCR. Electric car battery: An overview on global demand, recycling and future approaches towards sustainability. Journal of Environmental Management 2021;295:113091.
[3] Pordanjani AH, Aghakhani S, Afrand M, Zhang P, Tang R, Mahian O, Wongwises S, Rashidi MM. Thermo-electrochemical simulation of the cooling process in a compact battery pack considering various configurations. Journal of Power Sources 2023;553:232112.
[4] Mustafa J, Alqaed S, Sharifpur M. Numerical study on performance of double-fluid parabolic trough solar collector occupied with hybrid non-Newtonian nanofluids: Investigation of effects of helical absorber tube using deep learning. Engineering Analysis with Boundary Elements 2022;140:562–80.
[5] Azizi Z, Barzegarian R, Behvandi M. Design-expert aided thermohydraulic assessment of a nanofluid-cooled cylindrical microchannel heat sink: Possible application for thermal management of electric vehicle batteries. Sustainable Energy Technologies and Assessments 2022;50:101876.
[6] Hamed MM, El-Tayeb A, Moukhtar I, El Dein AZ, Abdelhameed EH. A review on recent key technologies of lithium-ion battery thermal management: External cooling systems. Results in Engineering 2022;16:100703.
[7] He L, Jing H, Zhang Y, Li P, Gu Z. Review of thermal management system for battery electric vehicle. Journal of Energy Storage 2023;59:106443.
[8] García A, Monsalve-Serrano J, Sari RL, Martínez-Boggio S. Thermal runaway evaluation and thermal performance enhancement of a lithium-ion battery coupling cooling system and battery sub-models. Applied Thermal Engineering 2022;202:117884.
[9] Xu J, Chen Z, Qin J, Minqiang P. A lightweight and low-cost liquid-cooled thermal management solution for high energy density prismatic lithium-ion battery packs. Applied Thermal Engineering 2022;203:117871.
[10] Jetybayeva A, Aaron DS, Belharouak I, Mench MM. Critical review on recently developed lithium and non-lithium anode-based solid-state lithium-ion batteries. Journal of Power Sources 2023;566:232914.
[11] Abu SM, Hannan MA, Hossain Lipu MS, Mannan M, Ker PJ, Hossain MJ, Mahlia TMI. State of the art of lithium-ion battery material potentials: An analytical evaluations, issues and future research directions. Journal of Cleaner Production 2023;394:136246.
[12] Nasajpour-Esfahani N, Garmestani H, Rozati M, Smaisim GF. The role of phase change materials in lithium-ion batteries: A brief review on current materials, thermal management systems, numerical methods, and experimental models. Journal of Energy Storage 2023;63:107061.
[13] Chen H, Abidi A, Hussein AK, Younis O, Degani M, Heidarshenas B. Investigation of the use of extended surfaces in paraffin wax phase change material in thermal management of a cylindrical lithium-ion battery: Applicable in the aerospace industry. Journal of Energy Storage 2022;45:103685.
[14] Jiang Y, Wang X, Mahmoud MZ, Elkotb MA, Baloo L, Li Z, Heidarshenas B. A study of nanoparticle shape in water/alumina/boehmite nanofluid flow in the thermal management of a lithium-ion battery under the presence of phase-change materials. Journal of Power Sources 2022;539:231522.
[15] Mustafa J. Numerical investigation of the effect of inlet dimensions air duct and distance of battery packs for thermal management of three lithium-ion battery packs. Journal of Energy Storage 2022;48:103959.
[16] Samimi F, Babapoor A, Azizi M, Karimi G. Thermal management analysis of a Li-ion battery cell using phase change material loaded with carbon fibers. Energy 2016;96:355–71.
[17] Li MD, Liang P. Simulation Analysis of Battery Thermal Management System Using Phase Change Material (PCM). Applied Mechanics and Materials, 433. Trans Tech Publ; 2013. p. 2107–12.
[18] Mustafa J, Alqaed S, Almehmadi FA, Sharifpur M. Effect of simultaneous use of water-alumina nanofluid and phase change nanomaterial in a lithium-ion battery with a specific geometry connected solar system. Journal of Power Sources 2022;539:231570.
[19] Jilte R, Afzal A, Panchal S. A novel battery thermal management system using nano-enhanced phase change materials. Energy 2021;219:119564.
[20] El Idi MM, Karkri M, Abdou Tankari M. A passive thermal management system of Li-ion batteries using PCM composites: Experimental and numerical investigations. International Journal of Heat and Mass Transfer 2021;169:120894.
[21] Xie YQ, Song J, Chi PT, Yu JZ. Performance enhancement of phase change thermal energy storage unit using fin and copper foam. Applied Mechanics and Materials, 260. Trans Tech Publ; 2013. p. 137–41.
[22] Mousavi M, Hoque S, Rahnamayan S, Dincer I, Naterer GF. Optimal design of an air-cooling system for a Li-Ion battery pack in Electric Vehicles with a genetic algorithm. In: 2011 IEEE Congress of Evolutionary Computation (CEC); 2011. p. 1848–55.
[23] Ren R, Zhao Y, Diao Y, Liang L, Jing H. Active air cooling thermal management system based on U-shaped micro heat pipe array for lithium-ion battery. Journal of Power Sources 2021;507:230314.
[24] Chen F, Huang R, Wang C, Yu X, Liu H, Wu Q, Qian K, Bhagat R. Air and PCM cooling for battery thermal management considering battery cycle life. Applied Thermal Engineering 2020;173:115154.
[25] Qin P, Liao M, Zhang D, Liu Y, Sun J, Wang Q. Experimental and numerical study on a novel hybrid battery thermal management system integrated forced-air convection and phase change material. Energy Conversion and Management 2019;195:1371–81.
[26] Deng T, Ran Y, Zhang G, Yin Y. Novel leaf-like channels for cooling rectangular lithium ion batteries. Applied Thermal Engineering 2019;150:1186–96.
[27] Doyle M, Newman J, Gozdz AS, Schmutz CN, Tarascon JM. Comparison of modeling predictions with experimental data from plastic lithium ion cells. Journal of The Electrochemical Society 1996;143:1890.
[28] Zhang X, Tang Y, Zhang F, Lee C-S. A Novel Aluminum–Graphite Dual-Ion Battery. Advanced energy materials 2016;6:1502588.
[29] Daneh-Dezfuli A, Pordanjani AH. Investigation of passive method in thermal management of lithium-ion batteries at different discharge rates by changing the number of cavities containing phase change materials. Journal of Energy Storage 2022;52:104758.
[30] Li L, Zhang D, Deng J, Gou Y, Fang J, Cui H, Zhao Y, Cao M. Carbon-based materials for fast charging lithium-ion batteries. Carbon 2021;183:721–34.
[31] Wang D, Wang X-X, Jin ML, He P, Zhang S. Molecular level manipulation of charge density for solid-liquid TENG system by proton irradiation. Nano Energy 2022;103:107819.
[32] Amiribavandpour P, Shen W, Mu D, Kapoor A. An improved theoretical electrochemical-thermal modelling of lithium-ion battery packs in electric vehicles. Journal of Power Sources 2015;284:328–38.
[33] Karimi G, Li X. Thermal management of lithium-ion batteries for electric vehicles. International Journal of Energy Research 2013;37:13–24.
[34] Nazer-Nejad M, Saffarian MR, Behbahani-Nejad M. Investigating the possibility of using the underground tunnel for air-conditioning in Tehran. Journal of the Brazilian Society of Mechanical Sciences and Engineering 2018;40:473.
[35] Biwole PH, Eclache P, Kuznik F. Phase-change materials to improve solar panel's performance. Energy and Buildings 2013;62:59–67.
[36] Li C, Cui N, Chang L, Cui Z, Yuan H, Zhang C. Effect of parallel connection topology on air-cooled lithium-ion battery module: Inconsistency analysis and comprehensive evaluation. Applied Energy 2022;313:118758.